Spin Dynamics Simulations

— *A Powerful Method for the Study of Critical Dynamics* —

D. P. Landau, Alex Bunker,*) Hans Gerd Evertz,**) M. Krech and Shan-Ho Tsai

Center for Simulational Physics, University of Georgia, Athens, GA 30602, USA

(Received October 31, 1999)

Spin-dynamics techniques can now be used to study the deterministic time-dependent behavior of magnetic systems containing over 10^5 spins with quite good accuracy. This approach will be introduced, including the theoretical foundations of the methods of analysis. Then newly developed, improved techniques based upon Suzuki-Trotter decomposition methods will be described. The current "state-of-the-art" will be evaluated with specific examples drawn from data on simple magnetic models. The examination of dynamic critical behavior will be highlighted but the extraction of information about excitations at low temperatures will be included.

§1. Introduction

The static behavior of physical systems near continuous phase transitions is characterized by a set of static critical exponents, which describe the critical behavior of thermodynamic quantities such as the specific heat, the order parameter, the correlation length, and so on. One can thus define different universality classes, within which the critical exponents are identical. The numerical values of the critical exponents depend only on the symmetry of the order parameter, the dimensionality of the system and the range of interactions, but not on either the precise form of the model Hamiltonian or the lattice type. Likewise, the dynamic critical behavior is describable in terms of a dynamic critical exponent z, which depends on the conservation laws and which, in analogy to static critical phenomena, gives rise to different dynamic universality classes.[1)] Our understanding of static critical behavior is now mature and has resulted largely from the investigation of simple model spin systems such as the Ising, the XY, and the Heisenberg model. These models are equally valuable for the investigation of dynamic critical behavior and dynamic scaling. Realistic models of magnetic materials can be constructed from these simple spin models; however, the theoretical analysis of experimentally accessible quantities, such as the dynamic structure factor, is usually too demanding for analytical methods. Computer simulations are beginning to provide important information about dynamic critical behavior and material properties of model magnetic systems.[2)-4)] These simulations use model Hamiltonians with continuous degrees of freedom represented by a three-component spin $\boldsymbol{S}_j$ with fixed length $|\boldsymbol{S}_j| = 1$ for each lattice

*) Present address: Max Planck Institute for Polymer Research, Ackermann Weg 10, Mainz D-55021-3148, Germany.

**) Present address: Inst. f. Theor. Physik, TU Graz, 8010 Graz, Austria.

site j. A typical model Hamiltonian is then given by

$$\mathcal{H} = -J \sum_{\langle j,l \rangle} \left(S_j^x S_l^x + S_j^y S_l^y + \lambda S_j^z S_l^z \right) - D \sum_j \left(S_j^z \right)^2, \tag{1·1}$$

where J is the coupling constant, $\langle j, l \rangle$ denotes a nearest-neighbor pair of spins, λ is an anisotropy parameter, and D determines the strength of a single-site or crystal field anisotropy. (We use units in which Boltzmann's constant $k_B = 1$.)

The dynamics of the spins are governed by the coupled equations of motion [5)]

$$\frac{d}{dt}\boldsymbol{S}_j = \frac{\partial \mathcal{H}}{\partial \boldsymbol{S}_j} \times \boldsymbol{S}_j, \tag{1·2}$$

and the time dependence of each spin can be determined from the integration of these equations, where (hybrid) Monte-Carlo simulations of the model provides *equilibrium* configurations as initial conditions for Eq. (1·2).

The most important quantity to be extracted from the numerical results is the dynamic structure factor $S(\boldsymbol{q}, \omega)$ for momentum transfer $\boldsymbol{q}$ and frequency transfer ω, which can be measured in neutron scattering experiments, and is given by

$$S^k(\boldsymbol{q}, \omega) = \sum_{\boldsymbol{R}} e^{i\boldsymbol{q}\cdot\boldsymbol{R}} \int_{-\infty}^{+\infty} e^{i\omega t} C^k(\boldsymbol{R}, t) \frac{dt}{\sqrt{2\pi}}, \tag{1·3}$$

where $\boldsymbol{R} = \boldsymbol{r}_j - \boldsymbol{r}_l$ ($\boldsymbol{r}_j$ and $\boldsymbol{r}_l$ are lattice vectors), $C^k(\boldsymbol{R}, t)$ is the space- and time-displaced correlation function, with $k = x, y$, or z, defined as $C^k(\boldsymbol{R}, t) = \langle {S_j}^k(t) {S_l}^k(0) \rangle - \langle {S_j}^k(t) \rangle \langle {S_l}^k(0) \rangle$.

Two practical limitations on spin-dynamics techniques are the finite lattice size and the finite evolution time. The finite time cutoff can introduce oscillations in $S^k(\boldsymbol{q}, \omega)$, which can be smoothed out by convoluting the spin-spin correlation function with a resolution function in frequency, which is equivalent to the energy resolution in neutron-scattering experiments, yielding $\bar{S}^k(\boldsymbol{q}, \omega)$. Finite-size scaling theory [3),6)] can be used to extract the dynamic critical exponent z: the divergence of the correlation length ξ is limited by L and the dynamic finite-size relations are given by

$$\frac{\omega \bar{S_L}^k(\boldsymbol{q}, \omega)}{\bar{\chi}_L^k(\boldsymbol{q})} = G^k(\omega L^z, qL, \delta_\omega L^z) \tag{1·4}$$

and

$$\bar{\omega}_m^k = L^{-z} \bar{\mathcal{W}}^k(qL, \delta_\omega L^z), \tag{1·5}$$

where $\bar{\chi}_L^k(\boldsymbol{q})$ is the total integrated intensity and $\bar{\omega}_m^k$ is a characteristic frequency, defined as

$$\int_{-\bar{\omega}_m^k}^{\bar{\omega}_m^k} \bar{S_L}^k(\boldsymbol{q}, \omega) \frac{d\omega}{2\pi} = \frac{1}{2} \bar{\chi}_L^k(\boldsymbol{q}). \tag{1·6}$$

To speed up the numerical integration of Eq. (1·2) it is desirable to use the largest possible time step; however, with standard methods the size of the time step is severely limited by the accuracy within which the *conservation laws* of the

dynamics are obeyed. It is evident from Eq. (1·2) that the total energy is conserved, and if, for example, $D = 0$ and $\lambda = 1$ (isotropic Heisenberg model) the magnetization $\boldsymbol{M} = \sum_j \boldsymbol{S}_j$ is also conserved. For the anisotropic Heisenberg model, i.e., $\lambda \neq 1$ or $D \neq 0$ only M_z is conserved. Conservation of spin length and energy is particularly crucial, because the condition $|\boldsymbol{S}_j| = 1$ is a major part of the definition of the model and the energy of a configuration determines its statistical weight. It would therefore also be desirable to devise an algorithm which conserves these two quantities *exactly*.

The remaining sections of this paper are organized as follows. In §2 we describe integration methods, including a newly developed technique based on Suzuki-Trotter decompositions of exponential operators.[7),8)] In §3 we discuss two examples of physical systems, namely the two-dimensional XY model and the three-dimensional Heisenberg antiferromagnet, and comparison with experiment and theory. The purpose of these examples is to show just how far the state-of-the-art has developed in producing and analyzing spin-dynamics data. In §4 we give a brief summary of this paper.

§2. Integration methods

2.1. *Predictor-corrector method*

Predictor-corrector methods have been quite effective for the numerical integration of spin equations of motion; however, in order to limit truncation errors small time steps δt must be used with at least a 4th-order scheme. The predictor step of the scheme used here is the explicit Adams-Bashforth four-step method[9)] and the corrector step consists of typically one iteration of the implicit Adams-Moulton three-step method.[9)] This predictor-corrector method is very general and is independent of the special structure of the equations of motion (see Eq. (1·2)). The conservation laws discussed earlier will only be observed within the accuracy set by the truncation error of the method. In practice, this limits the time step to typically[4)] $\delta t = 0.01/J$ in $d = 3$, where the total integration time is typically $600/J$ or less.

2.2. *Suzuki-Trotter decomposition methods*

The motion of a spin may be viewed as a precession of the spin $\boldsymbol{S}$ around an effective axis Ω which is itself time dependent. The lattice can be decomposed into two sublattices such that a spin on one sublattice precesses in a local field Ω of neighbor spins which are *all* located on the other sublattice. For the Hamiltonian in Eq. (1·1) there are only two such sublattices if the underlying lattice is simple cubic.

To illustrate the method, we consider first the $D = 0$ case. The basic idea of the algorithm is to rotate a spin about its local field Ω by an angle $\alpha = |\Omega|\delta t$, rather than directly integrate Eq. (1·2). This procedure guarantees the conservation of the spin length $|\boldsymbol{S}|$ and energy to within machine accuracy. Denoting the two sublattices by $\mathcal{A}$ and $\mathcal{B}$, respectively, we can express the local fields acting on the spins on sublattice $\mathcal{A}$ and $\mathcal{B}$ as $\Omega_{\mathcal{A}}[\{\boldsymbol{S}\}]$ and $\Omega_{\mathcal{B}}[\{\boldsymbol{S}\}]$, respectively. In a more symbolic way, we denote y as a complete spin configuration, which is decomposed into two sublattice components

$y_{\mathcal{A}}$ and $y_{\mathcal{B}}$, i.e. $y = (y_{\mathcal{A}}, y_{\mathcal{B}})$, and we denote by matrices A and B the generators of the rotation of the spin configuration $y_{\mathcal{A}}$ on sublattice $\mathcal{A}$ at fixed $y_{\mathcal{B}}$ and of the spin configuration $y_{\mathcal{B}}$ on sublattice $\mathcal{B}$ at fixed $y_{\mathcal{A}}$, respectively. The update of the configuration y from time t to $t+\delta t$ is then given by an exponential (matrix) operator

$$y(t+\delta t) = e^{(A+B)\delta t} y(t). \tag{2·1}$$

The exponential operator in Eq. (2·1) rotates each spin of the configuration and it has no simple explicit form, because the rotation axis for each spin depends on the configuration itself; however, the set of equations of motion for spins on one sublattice reduces to a *linear* system of differential equations if the spins on the other sublattice are kept fixed and the operators $e^{A\delta t}$ and $e^{B\delta t}$ which rotate $y_{\mathcal{A}}$ at fixed $y_{\mathcal{B}}$ and $y_{\mathcal{B}}$ at fixed $y_{\mathcal{A}}$, respectively, *do* have a simple explicit form. [8] Thus an *alternating* update scheme may be used, i.e., we rotate $y_{\mathcal{A}}$ at fixed $y_{\mathcal{B}}$ and vice-versa. The alternating update scheme amounts to the replacement $e^{(A+B)\delta t} \to e^{A\delta t} e^{B\delta t}$ in Eq. (2·1), which is only correct [10] up to order $(\delta t)^2$. The magnetization will therefore only be conserved up to terms of the order δt (global truncation error). To decrease truncation error and thus to improve the conservation, one can employ mth-order Suzuki-Trotter decompositions of the exponential operator in Eq. (2·1), namely [10]

$$e^{(A+B)\delta t} = \prod_{i=1}^{u} e^{p_i A\delta t/2} e^{p_i B\delta t} e^{p_i A\delta t/2} + \mathcal{O}(\delta t^{m+1}), \tag{2·2}$$

where $u = 1$ for 2nd-order, $u = 5$ for 4th-order, and $u = 15$ for 8th-order and the parameters p_i are given by Suzuki and Umeno. [10]

The additional computational effort needed to evaluate higher order expressions can be compensated to some extent by using larger time steps. The inclusion of next-nearest neighbor bilinear interactions on a simple cubic lattice can be treated within the above framework if the lattice is decomposed into four sublattices.

This approach can also be extended to the case $D \neq 0$, but in contrast to the isotropic case, the equation of motion for each individual spin on each sublattice is *nonlinear*. In practice, the best form of solution is via iterative numerical methods. In order to perform a rotation operation in analogy to the isotropic case we identify an effective rotation axis $\widetilde{\Omega}_j = \Omega_j - D\left(0, 0, S_j^z(t) + S_j^z(t+\delta t)\right)$, such that the condition for energy conservation is rewritten in the form $\widetilde{\Omega}_j \cdot (\boldsymbol{S}_j(t+\delta t) - \boldsymbol{S}_j(t)) = 0$. Since the rotation requires knowledge of S_j^z at the future time $t+\delta t$, we use an iterative procedure starting from the initial value $S_j^z(t+\delta t) = S_j^z(t) + (\Omega_j \times S_j(t))^z \delta t$ and performing several updates according to the decompositions given by Eq. (2·2) in order to improve energy conservation. Both the degree of conservation and the execution time depend to some extent on the number of iterations used.

For a quantitative analysis of the integration methods outlined above we restrict ourselves to the Hamiltonian given by Eq. (1·1) for $\lambda = 1$ in $d = 3$ and $J > 0$. The underlying lattice is simple cubic with $L = 10$ lattice sites in each direction and periodic boundary conditions. In order to compare the different integration methods we investigate the accuracy within which the conservation laws are fulfilled. The initial configuration is a well equilibrated one from a Monte-Carlo simulation

for $\lambda = 1$ at a temperature $T = 0.8T_c$ for $D = 0$ and $D = J$, where T_c refers to the critical temperature of the isotropic model ($D = 0$). Figure 1 shows the magnetization conservation for the 4th- and 8th-order decomposition methods, both with $\delta t = 0.1/J$, for $D = 0$ and Fig. 2 shows the energy conservation for different methods for $D = J$. In the latter case the iterative nature of all four methods gives rise to a basically linear energy change. A single integration step using the 2nd-, the 4th- and the 8th-order scheme is respectively about 2 times faster, 2.5 and 9 times slower than the predictor-corrector method; the speedup of the decomposition

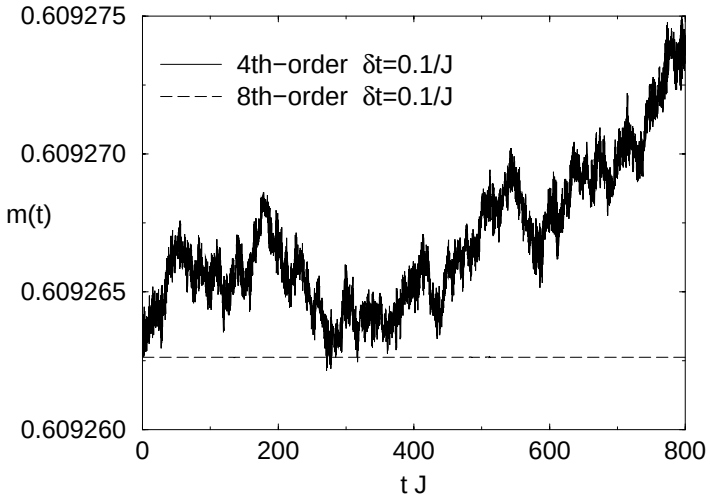

Fig. 1. Magnetization $m(t) = |\boldsymbol{M}(t)|/L^3$ per spin for different order decomposition schemes for $D = 0$ and time step $\delta t = 0.1/J$: (solid line) 4th-order scheme; (dashed line) 8th-order method.

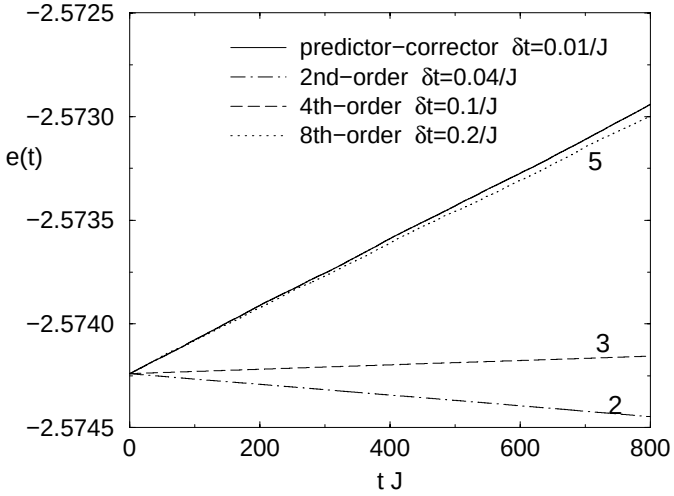

Fig. 2. Energy $e(t) = E(t)/(JL^3)$ per spin for different order decomposition schemes for $D = J$: (solid line) predictor-corrector method; (dot-dashed line) 2nd-order scheme; (dashed line) 4th-order scheme; (dotted line) 8th-order method. The number of iterations performed are marked next to each line.

methods comes from the much larger δt that can be used. For $D = 0$ it is still feasible to use the 4th-order method with $\delta t = 0.2/J$, which corresponds to an eightfold speedup as compared to the predictor-corrector method. The 8th-order method improves the conservation significantly but at the cost of greatly increased execution time.

§3. Examples of physical systems

3.1. *Two-dimensional XY model*

The two-dimensional XY model can be described by the Hamiltonian in Eq. (1·1) with $\lambda = 0$ and $D = 0$. At the critical temperature [2] $T_{KT} = 0.700(5)J$, the model undergoes an unusual phase transition to a state with bound, topological excitations (vortex pairs), and the static properties are consistent with the predictions of the Kosterlitz-Thouless theory. [11] For $T \leq T_{KT}$ the model is critical, i.e. the correlation length is infinite, but there is no long-range order, and the spin-spin correlation function decays algebraically with distance, with an exponent η that varies with temperature.

In our studies of the dynamics of this model, [2] we used $L \times L$ lattices with periodic boundary conditions for $16 \leq L \leq 192$ and several values of T. The equations of motion (see Eq. (1·2)) were integrated using a 4th-order predictor-corrector method, with a time step of $\delta t = 0.01/J$, to a maximum time $t_{\max} = 400/J$. Between 500 and 1200 equilibrium configurations were used for each lattice size and temperature. We were limited to the [10] reciprocal lattice direction, i.e. $\boldsymbol{q} = (q, 0)$ and $(0, q)$.

For $T \leq T_{KT}$, the in-plane component $S^x(q, \omega)$ exhibits very strong and sharp spin-wave peaks. As T increases, they widen slightly and move to lower ω, but remain pronounced even just above T_{KT}. For increasing momentum they broaden and rapidly lose intensity. Well above T_{KT}, the spin-wave peak disappears in $S^x(q, \omega)$, as

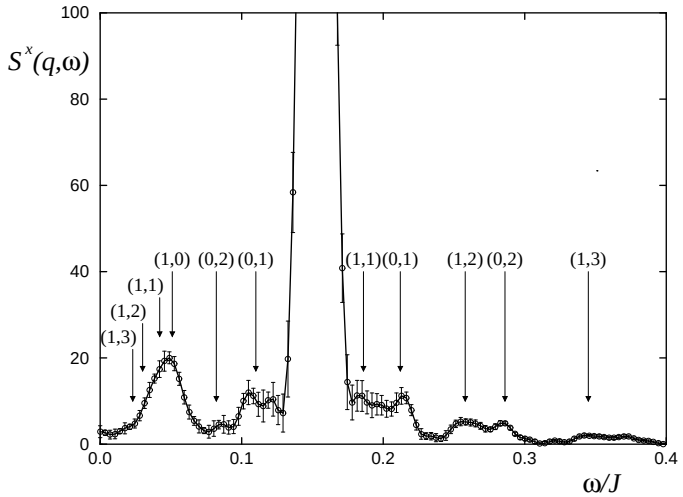

Fig. 3. Low-intensity structure in $S^x(q, \omega)$ for $T = 0.6J, L = 192$ and $q = \pi/32$. Vertical arrows show the location of two-spin-wave peaks formed by spin waves of small momentum $q < 4(2\pi/L)$.

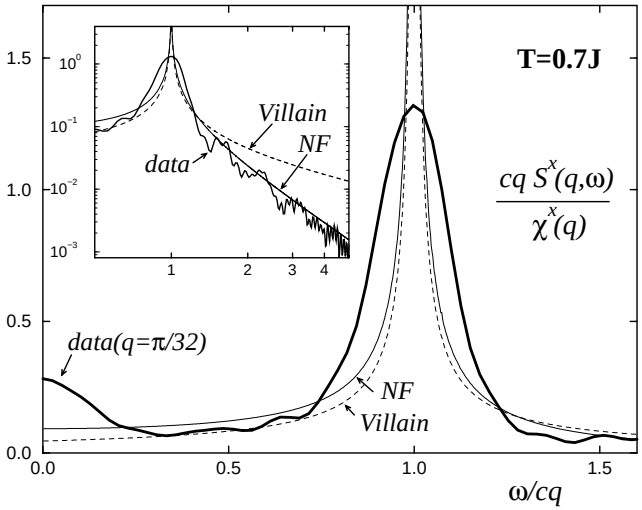

Fig. 4. Comparison of the line shape of $S^x(q,\omega)$ with theoretical predictions. Data are at $T = T_{KT}$, $L = 128$, and $q = \pi/32$ (thick line), normalized as $cqS^x(q,\omega)/\chi^x(q)$, where c is the spin-wave velocity. The two thin lines represent the predictions by Nelson and Fisher [13] (continuous line) and by Villain [12] (dashed line), both with $\eta = 0.25$. The inset shows the data and predictions on a log-log plot that includes large values of ω.

expected, and we observe a large central peak instead. Besides the spin-wave peak, $S^x(q,\omega)$ exhibits a rich low-intensity structure, which we interpret as two-spin-wave processes (see Fig. 3). Furthermore, $S^x(q,\omega)$ shows a clear central peak, even below T_{KT}, which becomes very pronounced towards T_{KT}. Neither this strong central peak nor the additional structure are predicted by existing analytical calculations. The out-of-plane component $S^z(q,\omega)$ is much weaker than $S^x(q,\omega)$, except for large q. The very sharp spin-wave peaks at low temperatures allowed us to determine the dispersion curves with great accuracy. Our estimated value of the dynamic critical exponent is $z = 1.00(4)$, in agreement with the theoretical prediction of $z = 1$. The line shape of $S^x(q,\omega)$ is not well described by either Villain's [12] or Nelson and Fisher's [13] prediction (the latter agrees qualitatively with our data only for large q) (see Fig. 4). Moreover, these predictions do not describe the additional structure in $S^x(q,\omega)$, including the central peak.

3.2. *Three-dimensional Heisenberg antiferromagnet and $RbMnF_3$*

$RbMnF_3$ is a good physical realization of an isotropic three-dimensional Heisenberg antiferromagnet, described by the Hamiltonian in Eq. (1·1) with $\lambda = 1$, $D = 0$ and $J < 0$. Early experimental studies [see references in Ref. 14)] showed that the Mn^{2+} ions, with spin $S = 5/2$, form a simple cubic lattice structure with a nearest-neighbor exchange constant $|J^{\exp}| = 0.58(6)$ meV and a second-neighbor interaction constant of less than 0.04 meV, both defined using the normalization as in Eq. (1·1). Magnetic ordering with antiferromagnetic alignment of spins occurs below the critical temperature $T_c = 83\,\mathrm{K}$. The magnetic anisotropy is very low, about 6×10^{-6} of the exchange field, and no deviation from cubic symmetry was seen at T_c.

In our simulations,[14] we used simple cubic lattices with $12 \leq L \leq 60$ at $T \leq T_c = 1.442929(77)|J|$. Numerical integrations of the coupled equations of motion were performed to a maximum time $t_{\max} \leq 1000|J|^{-1}$, using the algorithm based on 4th-order Suzuki-Trotter decompositions of exponential operators, with a time step $\delta t = 0.2|J|^{-1}$. As many as 7000 initial configurations were used, although for large lattices this was reduced to as few as 400. We were limited to the [100], [110] and [111] directions, i.e. $\boldsymbol{q} = (q, 0, 0)$, $(q, q, 0)$, (q, q, q) and the equivalent momenta. For this model the order parameter is not conserved and the dynamic structure factor

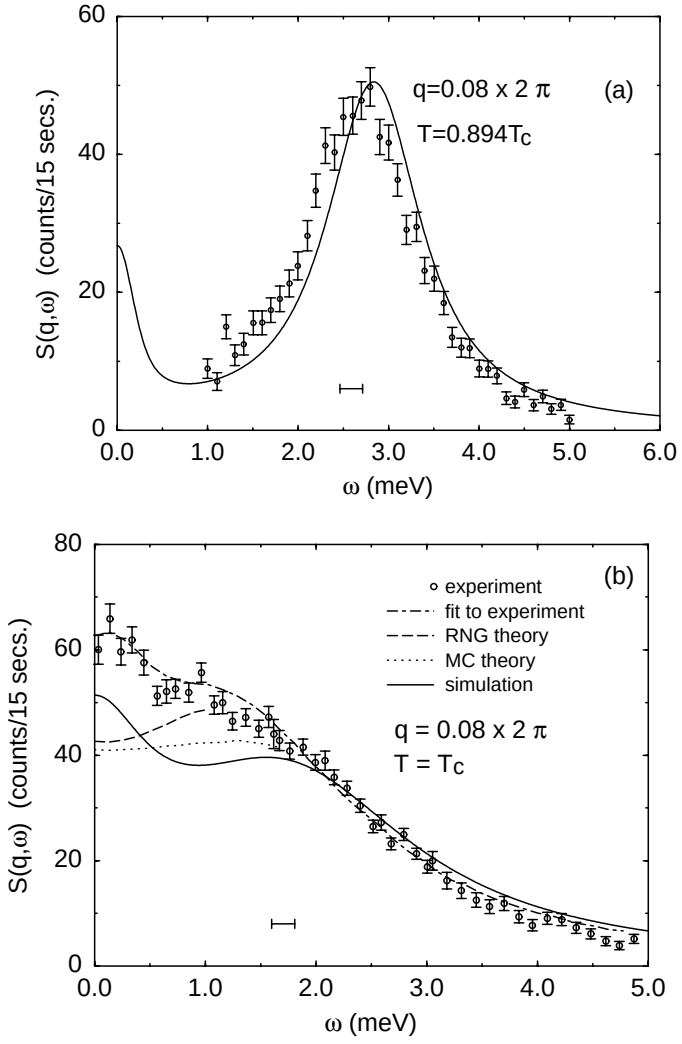

Fig. 5. Comparisons of lineshapes obtained from fits to simulation data for $L = 60$ (solid line) and the experiment (open circles) for $q = 2\pi(0.08)$ in the [111] direction, at (a) $T = 0.894T_c$ and (b) $T = T_c$. The dot-dashed line in (b) is a fit to the experimental data which is compared to the predictions of renormalization group (RNG) and mode coupling (MC) theory. The horizontal line segment in each graph represents the 0.25meV resolution in energy (full-width at half-maximum).

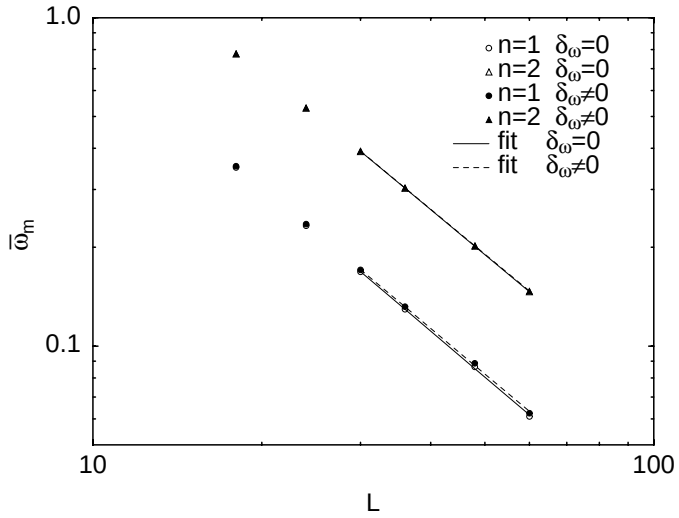

Fig. 6. Finite-size scaling plot for $\bar{\omega}_m$ (with qL =const, $\delta_\omega L^z$ =const) for the analysis with and without a resolution function. For the former case, the data used correspond to the converged values of z, for $n = 1, 2$. The error bars were smaller than the symbol sizes.

cannot be separated into a longitudinal and a transverse component. Henceforth we will use the term dynamic structure factor $S(q, \omega)$ and characteristic frequency $\bar{\omega}_m$ to refer to the average.

We compare our results with the recent neutron scattering data of Coldea et al. [15] Although the compound $RbMnF_3$ is a quantum system, and our simulations are for a classical Hamiltonian, it has been shown that quantum Heisenberg systems with large spin values ($S \geq 2$) behave as classical Heisenberg systems where the spins are vectors of magnitude $\sqrt{S(S+1)}$ with the same interaction strength. Since our classical spins were vectors of unit length, to preserve the Hamiltonian and the dynamics, a normalization of the interaction strength and the frequency transfer are needed, i.e. $J = J^{\rm exp} S(S+1)$ and $\omega^{\rm exp} = J^{\rm exp}\sqrt{S(S+1)}\, w/J$. For our comparison, the experimental T- and ω-dependent population factor was removed from the experimental data, and the lineshapes from our simulation were convoluted with the experimental Gaussian resolution function in energy. Figure 5 shows the direct comparison of $S(q, \omega)$ in the [111] direction from simulation and experiment for $q = 2\pi(0.08)$ [in this notation the Brillouin zone edge in the [111] direction corresponds to $q = 2\pi(0.25)$], at $T = 0.894 T_c$ and at T_c. Below T_c, renormalization group theory [16] (RNG) predicts a spin-wave peak and a central peak in the longitudinal component of $S(q, \omega)$; however, at T_c, both RNG [17] and mode coupling [18] (MC) theory predict only the presence of a spin-wave peak, while the experiment and the simulation find a spin-wave peak and a central peak at $T = T_c$ as well (see Fig. 5(b)). At low temperatures the central peak has very low intensity and the dominant structures are very narrow and sharp spin-wave peaks, from which accurate dispersion curves could be found. The dispersion curve for small q changes from a linear behavior at low T to a power-law relation as $T \to T_c$.

The dynamic critical exponent z was extracted from the slope of a $\log(\bar{\omega}_m)$ vs $\log(L)$ plot (see Eq. (1·5)) corresponding to the [100] direction, using lattices in the asymptotic-size regime ($L \geq 30$), and keeping qL and $\delta_\omega L^z$ constant. For $\delta_\omega = 0$, we find $z = 1.45(1)$ for $n = qL/(2\pi) = 1$ and $z = 1.42(1)$ for $n = 2$. Using $\delta_\omega \neq 0$ requires an iterative procedure and the converged values that we obtained are $z = 1.43(1)$ for $n = 1$ and $z = 1.42(1)$ for $n = 2$. Hence, our final estimate is $z = 1.43(3)$, which is in agreement with the recent experimental value $z = 1.43(4)$, and slightly lower than the theoretical prediction $z = d/2 = 1.5$.

§4. Summary

We have shown how spin-dynamics techniques can be used to study critical and low-temperature magnetic excitations using simple classical spin models that have true dynamics, governed by equations of motion. The solution of these equations is generally possible through the use of algorithms based on Suzuki-Trotter decompositions of exponential operators and we compare their relative performance with each other and with a predictor-corrector method. As examples of interesting physical systems, we studied the two-dimensional XY model and the three-dimensional Heisenberg model. We determined dynamic structure factors and through a finite-size scaling we estimated the dynamic critical exponent of these systems. We have also made comparisons with theoretical predictions and experimental data.

Acknowledgements

This work was partially supported by NSF grant No. DMR-9727714. Our simulations were carried out on the Cray T90 at the San Diego Supercomputing Center, and on an SGI Origin2000 and IBM R6000 in the University of Georgia.

References

1) P. C. Hohenberg and B. I. Halperin, Rev. Mod. Phys. **49** (1977), 435.
2) H. G. Evertz and D. P. Landau, Phys. Rev. **B54** (1996), 12302.
3) K. Chen and D. P. Landau, Phys. Rev. **B49** (1994), 3266.
4) A. Bunker, K. Chen and D. P. Landau, Phys. Rev. **B54** (1996), 9259.
5) R. W. Gerling and D. P. Landau, Phys. Rev. **B41** (1990), 7139.
6) D. C. Rapaport and D. P. Landau, Phys. Rev. **E53** (1996), 4696.
7) F. Frank, W. Huang and B. Leimkuhler, J. Comp. Phys. **133** (1997), 160.
8) M. Krech, A. Bunker and D. P. Landau, Comput. Phys. Commun. **111** (1998), 1.
9) R. L. Burden, J. D. Faires and A. C. Reynolds, *Numerical Analysis* (Prindle, Weber & Schmidt, Boston, 1981), p. 205, p. 219.
10) M. Suzuki and K. Umeno in *Computer Simulation Studies in Condensed Matter Physics VI*, ed. D. P. Landau, K. K. Mon and H. B. Schüttler (Springer, Berlin, 1993), p. 74.
11) J. M. Kosterlitz and D. J. Thouless, J. of Phys. **C6** (1973), 1181.
12) J. Villain, J. de Phys. **35** (1974), 27.
13) D. R. Nelson and D. S. Fisher, Phys. Rev. **B16** (1977), 4945.
14) S.-H. Tsai, A. Bunker and D. P. Landau, Phys. Rev. B, in press (see references therein).
15) R. Coldea, R. A. Cowley, T. G. Perring, D. F. McMorrow and B. Roessli, Phys. Rev. **B57** (1998), 5281.
16) G. F. Mazenko, M. J. Nolan and R. Freedman, Phys. Rev. **B18** (1978), 2281.
17) R. Freedman and G. F. Mazenko, Phys. Rev. Lett. **34** (1975), 1575; Phys. Rev. **B13** (1976), 4967.
18) A. Cuccoli, S. W. Lovesey and V. Tognetti, J. of Phys.: Cond. Matt. **6** (1994), 7553.